5-7-2016

Differential Gene Expression in TRAP-positive Cells During Mouse Embryonic Skeletal Development

Melissa Carr-Reynolds
UConn Health, carrreynolds@uchc.edu

Differential Gene Expression in TRAP-positive Cells During Mouse Embryonic Skeletal Development

Melissa Carr-Reynolds

B.S., Spelman College, 2014

A Thesis

Submitted in Partial Fulfillment of the

Requirements for the Degree of

Master of Science Thesis

At the

University of Connecticut

2016

APPROVAL PAGE

Master of Science Thesis

Differential Gene Expression in TRAP-positive Cells During Mouse Embryonic Skeletal Development

Presented by

Melissa Carr-Reynolds, B.S.

Major Advisor_____
Marc Hansen

Associate Advisor_____
Hicham Drissi

Associate Advisor_____
Anne Delany

University of Connecticut

2016

ACKNOWLEDGMENTS

This thesis is written in dedication to my Family: Arlene (mom), Christopher (dad), Lovinia (sister), and Austin (brother)…and of course to my two favorite pets, Sable (the family poodle) and Creamsickle (my guinea pig).

I am so grateful to my mentor and advisor, Marc Hansen, who has guided and taught me so much over the past year and a half.

A special thank you to the members of the Young Innovative Investigator Program (YIIP) and the Connecticut Institute for Clinical and Translational Science (CICATS), who funded the YIIP Program.

TABLE OF CONTENTS

FIGURES AND TABLES

ABSTRACT

The skeleton is formed via intramembranous ossification and endochondral ossification. Endochondral ossification, which is the focus of this research, is the process by which the long bones of the skeleton undergo chondrogenesis followed by osteogenesis. The objective of this project is to define the genetic profiles of two types of clastic cells in endochondral ossification: osteoclasts and chondroclasts, which are responsible for breaking down bone and calcified cartilage, respectively. The goal of this project is to validate the hypothesis that these two very similar cells types, which arise from a common precursor, are distinguished by a pattern of differentially expressed genes in response to the interaction with the two different microenvironments in which these cells are found. In order to carry out this experiment, E18.5 embryos were sectioned and stained for tartrate-resistant acid phosphatase (TRAP). TRAP-positive cells were captured using laser capture microdissection. Cells were then lysed so that the RNA could be isolated and transcribed to cDNA, which was linearly amplified, so that qPCR could be performed. A list of candidate genes was chosen for qPCR analysis. Results indicated that there are differences in the expression profiles between chondroclasts and osteoclasts. These results supported the hypothesis that chondroclasts and osteoclasts have distinct genomic profiles at timepoint E18.5 during embryonic development. Identifying and testing the functional differences in the genomic profile of these two cell types will be instrumental in developing new strategies to target these cells in diseases such as osteoarthritis and osteoporosis.

INTRODUCTION

Skeletal Formation During Embryogenesis

Skeletal development during embryogenesis requires the coordination of multiple programs including cellular growth, differentiation, apoptosis, extracellular matrix remodeling, and angiogenesis. The skeleton is formed via two processes: intramembranous ossification and endochondral ossification. The flat bones of the skull, scapulae, pelvic bone are formed through intramembranous ossification while the appendicular and axial skeleton are formed through endochondral ossification. These two processes both begin with the differentiation of mesenchymal stem cells. Mesenchymal stem cells are multipotent cells that can differentiate into many different cell lineages (i.e. bone, fat, muscle, cartilage, tendon and marrow stroma) (1). In both intramembranous and endochondral ossification, the mesenchymal stem cells first aggregate at the location of the future skeleton, to form mesenchymal condensations. In intramembranous ossification, the mesenchymal stem cells are derived from the neural crest of the cranium. The cranial neural crest-derived mesenchymal stem cells proliferate and are condensed into nodules and differentiate into osteoblasts. During this process, the osteoblasts also secrete a collagen-proteoglycan matrix that becomes calcified and vascularized and ultimately forms the osteoid matrix (2).

Endochondral ossification is the process by which the long bones of the skeleton are formed. Unlike intramembranous ossification, bones formed by endochondral ossification undergo a chondrogenic stage as well as an osteogenic stage. Thus endochondral ossification presents an orderly progression during which cartilage, which is a predominantly avascular tissue is replaced by bone, which is one of the most highly vascularized tissues in the body. In endochondral ossification during development, mesenchymal stem cells condense at sites that will eventually form the appendicular skeleton. These condensations take the form of the bones that will develop at these sites. Shortly after the condensation, the mesenchymal stem cells

undergo differentiation along the chondrogenic pathway to form chondrocytes. The resulting cartilaginous bone templates are called anlagen. The chondrocytes in the anlagen then undergo a further differentiation resulting in hypertrophy, which is marked by the expression of Type 10 collagen. The hypertrophic chondrocytes become surrounded by a calcified extracellular matrix, which is invaded by blood vessels from the perichondrium. At this time, another type of cell is recruited to the bone, a clastic cell that differentiates from the hematopoietic stem cells through the monocyte/macrophage lineage. Following this vascular invasion, the hypertrophic chondrocytes die through apoptosis and pre-osteoblasts, which also develop from the mesenchymal stem cells in the perichondrium adjacent to the hypertrophic chondrocytes differentiate and become osteoblasts. These osteoblasts deposit the bony extracellular matrix to generate the bone collar, whose extracellular matrix is characterized by Type I collagen, which again becomes calcified. At the same time that these osteoblasts stay on the periphery of the bone, others migrate into the center of the anlagen to form the beginning of the primary spongiosa, the precursor of trabecular bone.

This process of primary ossification, whereby osteoblasts replace chondrocytes, proceeds down the bone until the only remaining chondrocytes are confined to the growth plate at the ends of the bone. During this time, other clastic cells that arise from the monocyte/macrophage lineage are recruited to the developing bone and begin to break down the bony extracellular matrix in the process of bone remodeling, which will continue throughout the life of the animal. This remodeling of the bony matrix results in a cavity filled with vascular channels containing hematopoietic cells.

The timing of this whole ossification process is relatively rapid. In the mouse, the hyaline cartilage begins to form around embryonic day E12.5. At around E14.5, the hyaline cartilage begins to undergo proliferation and form the anlagen model of the bone. Chondrocytes in the anlagen then undergo hypertrophy and the differentiated chondrocytes eventually form the cartilaginous matrix. At around E16.5 this matrix then gets invaded by blood vessels, osteoclasts,

bone marrow cells and osteoblast precursor cells to form the primary ossification center (3). As the cartilage matrix gets removed by clastic cells, osteoblasts lay down bone in place of the cartilage and the primary ossification center expands away from the mid-shaft of the bone (4) at E18.5. Finally at around E20.5, immediately before birth, the remaining cartilage is restricted to the articular cartilage and the epiphyseal growth plate.

Osteoclasts and Chondroclasts: Cells that Break Down Mineralized Matrix

My research focuses on the cells that resorb mineralized matrix of hard tissues, otherwise known as clastic cells. Clastic cells, which include osteoclasts and chondroclasts, are responsible for breaking down bone and calcified cartilage, respectively. Clastic cells arise from pluripotent hematopoietic stem cells, which differentiate to form myeloid stem cells, which then differentiate and proliferate into granulocytes, monocytes and megakaryocytes (5). Of these myeloid stem cells, granulocytes (which are granulocyte-macrophage colony-forming cells) are the earliest hematopoietic precursor to the clastic cells (6). Of the two types of clastic cells, osteoclasts are more well-known and well-studied. Osteoclasts are characterized as giant, multinucleated cells required for maintaining bone homeostasis (7)**.** In order for osteoclasts to mature and become active, they must be stimulated by cytokines known as receptor activator of nuclear factor kappa-B ligand (RANKL) and macrophage colony stimulating factor (MCSF) (7, 8) RANKL, a regulatory receptor found on the surface of osteoblasts, interacts with its receptor RANK, found on the surface of osteoclasts and their progenitors, to initiate this process of osteoclastic differentiation. During the process of bone resorption, the clastic cell adheres to the bone surface and forms a microenvironment that is separate from the extracellular space. This isolation is carried out by what's known as the sealing zone. Adjacent to this sealing zone is the ruffled membrane or border (9). The ruffled border is a complex structure that is formed when lysosome-derived vesicles are inserted into the bone-apposed plasma membrane (10, 11)**.** It contains ions and charged channels that allow for the transport of acids such as HCl into the resorptive space,

which acidifies the bone area, releasing mineral, and exposes its organic matrix. This organic matrix is then degraded by Cathepsin K, another enzyme that is secreted from the ruffle border (9).

Chondroclasts: Clastic Cells that Resorb Cartilage Matrix

Chondroclasts, like osteoclasts, are multinucleated cells that appear on the surface of mineralized cartilage. In addition to being multinucleated, chondroclasts also express tartrate-resistant alkaline phosphatase (TRAP) activity and other cytokines such as metalloproteinase MMP9 and Cathepsin K (12). They also have ruffled-border membranes that are less developed than those of osteoclasts and are found on non-mineralized transversal septae whereas osteoclasts are found on mineralized longitudinal trabeculae (13). Previous research has identified chondroclasts and osteoclast as different cells that arose from the same hematopoietic precursor (14); however, their relationship to matrix resorbing cells and macrophages in development and diseased models (i.e. rheumatoid arthritis), is not well understood (15). There has also been debate as to whether chondroclasts are the same cells as osteoclasts or whether they are unique cells, separate from osteoclasts. Research performed by Knowles HJ 2012 suggested that chondroclasts and osteoclasts share many of the same phenotypic features (15). However another study suggested that chondroclasts and osteoclasts differ when semi-quantitative estimation of TRAP was performed in both cell types (16). These results showed an inverse relationship between the extracellular and intracellular TRAP in chondroclasts and osteoclasts (16). A third study observed chondroclasts in osteogenesis by implanting demineralized bone powder into the rectus abdominis of rats (17). This study found that giant polykarions in the implant after the cartilage matrix was calcified. They determined that these polykarions were chondroclasts resorbing cartilage (17). Despite these opposing views of chondroclasts, there is no doubt that they are cells that are intimately involved in endochondral ossification and are morphologically and histochemically similar to osteoclasts (12).

Work done previously by the Drissi/Hansen laboratories had examined the question of the similarity of the chondroclast and osteoclast during fracture healing (18). They determined that there were differences in patterns of genomic expression between chondroclasts and osteoclasts that were consistent with these two populations of TRAP-positive cells being distinct in the context of pathological fracture healing.

Defining the Chondroclast in Development

My research project focused on the process of endochondral ossification during mouse fetal development. In particular, my research tested whether the TRAP-positive cells found in the developing mineralized cartilage (chondroclasts) and in the developing mineralized bone (osteoclasts), during embryonic development, had similar or distinct gene expression profiles. While it is possible that the gene expression profiles of the chondroclast and osteoclast would be similar, it is also possible that these two cell types show distinct differences in expression based on their response to the cellular microenvironment that they encounter during endochondral ossification during development.

Hypothesis

My research hypothesizes that TRAP-positive chondroclasts and osteoclasts are distinct cell types that play different roles in skeletal development and are distinguished by unique patterns of differentially expressed genes. Identification of the genomic signatures of these two types of clastic cells can be used to examine the signals that cause a common precursor stem cell to give rise to these separate cell types. This difference in pattern of genomic expression profiles would likely reflect differences in the cellular microenvironment of the hypertrophic chondrocytes and the osteoblast. In turn, these experiments will allow us to identify genes that are important in defining the osteoclast and chondroclast cells in development.

MATERIALS AND METHODS

Timed Embryos/Samples:

E18.5 embryos were obtained courtesy of the H. Drissi and C. Dealy laboratories (19).

Embryonic Mouse Tissue Processing and Paraffin Embedding:

Using the Kosher and Dealy laboratories protocol, embryos were fixed in fresh-made paraformaldehyde in 1xPBS overnight at 4° C. All solutions were made in autoclaved DEPC water.

Embryos that are E16.5 and older must be decalcified after paraformaldehyde fixation at 4° C on a rocker. Embryos were first placed in PBS for 2 changes of 30 seconds then decalcified in 15% EDTA in PBS for 24 hours. They were then placed in PBS for 2 changes of 30 seconds, 0.9% NaCl for 2 changes of 30 seconds, 30% Ethanol for 1 hour, 50% Ethanol fo1 1 hour, and 70% for 1 hour. Embryos were stored in 70% Ethanol prior to processing.

Embryos were then processed in PBS for 2 changes of 30 seconds, 0.9% NaCl in DEPC water for 2 changes of 30 seconds, 30% Ethanol for 1 hour, 50% Ethanol fo1 1 hour, and 70% for 1 hour. Embryos were stored in 70% Ethanol in the freezer prior to paraffin embedding.

Paraffin embedding was done for E18.5 embryos in 95% Ethanol for 45 minutes, 100% Ethanol for 3 changes at 30 mins each, 100% Ethanol and Xylene for 30 minutes, Xylene for 3 changes at 30 minutes each, Xylene and Paraffin for 30 minutes and finally, in Paraffin for 4 changes at 45 minutes each under vacuum.

Immunohistochemistry & Immunocytochemistry:

Hematoxylin and Eosin (H&E) stain was used to identify clastic cells as multinucleated cells on sectioned embryos. The resulting stain showed the nuclei as blue and the cytoplasm as pink/red. I stained sections (7µm thick) from the femur and humerus of E18.5 embryos to identify

tartrate-resistant acid phosphatase (TRAP)-positive cells (*K-ASSAY*, Kamiya Biomedical Company). TRAP activity was detected using a colorimetric assay in which TRAP acts by cleaving the phosphate group from a substituted naphthol AS phosphate (Naphthol-AS-BI-phosphoric acid) to form naphthol-AS. This unstable product acts on a diazonium salt to generate an azoic dye which is deposited as a red stain on the TRAP-positive cells. Alcian Blue stain was used to counter-stain in order to identify hyaline and hypertrophic cartilage.

Laser Capture Microdissection:

It is critical that the chondroclast and osteoclast cells be collected as homogenous populations of cells. To do this, I used Laser Capture Microdissection (LCM) to capture individual cells from sections of the embryonic femur and humerus. LCM was performed with a PixCell II laser capture microdissection system (Life Technologies, Carlsbad, CA). Briefly, mouse embryos from 18.5dpc were collected, fixed in 4% formalin and embedded in paraffin. Serial 7µm sections were cut from each embryo and placed on uncharged microscope slides. The individual slides were stained for TRAP activity as discussed above. The slides were then serially dehydrated in 50% Ethanol for 5 minutes, 70% Ethanol for 5 minutes, 90% Ethanol for 10 minutes, 100% Ethanol 10 minutes and Xylene for 10 minutes. Laser capture microdissection was performed using a 7.5 µm laser spot with 100 mW power and 3.4 ms pulse duration. Individual TRAP-positive cells from the developing cartilage and developing bone were observed under 200X magnification and captured on Arcturus CapSure Macro LCM Caps (Life Technologies). Following capture, the individual caps were placed into Eppendorf tubes and stored at -20 degrees Celsius, until RNA isolation.

Lysis of RNA:

RNA was taken from each LCM cap containing 10 cells, either chondroclasts or osteoclasts. Capture and lysis was performed in triplicates using cells captured from different, wildtype

embryos. Since each capture involved only 10 cells, the amount of RNA to be isolated was very small. This required a number of steps, in which RNA lysis was followed by linear amplification of the RNA. RNA was lysed and amplified from the TRAP-positive cells using a modified version of the Single Cell Transcript Analysis, as previously described (20). Briefly, cells from each cap were lysed using 5% NP-40, RNAsin plus (Promega #N2611), PBS in the presence of a pool of gene-specific SYBR Green Primers (200 nM). Cells were denatured in thermocycler at 70 degrees Celsius for 10 minutes and 4 degrees Celsius for 5 minutes.

Reverse transcription:

The RNA was reversed transcribed using the ABI High Capacity cDNA Reverse Briefly, the transcription mixture included a 10X RT buffer, 25X dNTP mix (final concentration of 100 mM), 10X RT Random Primers, Multiscribe Reverse Transcriptase, RNAse Inhibitor and Nuclease free water. The reverse transcription was performed using a thermocycler with a program of 37 degrees Celsius for 2 minutes, 42 degrees Celsius for 1 min, 50 degrees Celsius for 40 cycles. The mixture was heated to 85 degrees Celsius for 5 minutes and held at 4 degrees Celsius and stored at -20.`.

Pre-Amplification:

Following lysis of the cells and reverse transcription of the RNA, it was necessary to linearly amplify the cDNA prior to analysis by qPCR. The cDNA pre-mixture was amplified using a Pool of SYBR Green primers (200 nM), UltraPure water, and Takara PCR Premix and Taq polymerase (#R004A). This was performed in a thermocycler with a program at 95 degrees Celsius for 3 minutes, 55 degrees for 2 minutes and 72 degrees Celsius for 2 minutes, then 95 degrees Celsius for 15 seconds, 60 degrees Celsius for 2 minutes and 72 degrees Celsius for 2 minutes for 16 cycles. Following the amplification, the mixture was held at 4 degrees Celsius and stored at -20.

RT-qPCR analysis:

During the process of formalin-fixation, paraffin-embedding followed by LCM extraction and cell lysis and RNA linear amplification, the amplified product was highly degraded to approximately 100-120 bps. This necessitated using specific primers for qPCR analysis (**Table 1**). The primer pairs needed to have an amplified product of about 100 nucleotides or less.

The linearly amplified cDNA was now ready for gene-specific qPCR. Briefly, a total of 4 µg of each triplicate amplified cDNA sample was used as template. A single qPCR master mix was prepared for each sample consisting of the 4 µg cDNA and iTaq Universal SYBR Green Supermix (Life Technologies, Grand Island, NY). 10 µl qPCR reactions consisting of approximately 20 ng of cDNA equivalent were run in 96-well plates using an Applied Biosystems 7500 Real-Time PCR System (Bio-Rad Laboratories).

Table 1: Genes and their Specific Primers

Gene	Amplicon size	Primer Bank ID	Sequence (F and R)
Ubiquitin	76	212275974c1	F: CCCACGTCGGAGAACTTAACA R: GACAAGCAGCCGGGATAGAAG
Sp7	93	148747346c2	F: TCCCTGGATATGACTCATCCCT R: CCAAGGAGTAGGTGTGTTGCC
COL10A1	77	158187527c3	F: GGGACCCCAAGGACCTAAAG R: GCCCAACTAGACCTATCTCACCT
Gapdh	83	6679938c3	F: TTGTCATGGGAGTGAACGAGA R: CAGGCAGTTGGTGGTACAGG
Zfp595	102	29244006a1	F: GGGGGAAAAGCTATACGTGTAAA R: ACTTGCAGGACTTCACTCCTAAA
Higd2a	78	146135032c1	F: CCCCAGTTATCGAGGGCTTC R: GGGTCTTGCGAATAAACTTTTCC
Psmb9	106	118129789c3	F: ACCGTGAGGACTTGTTAGCG R: GTAAAGGGCTGTCGAATTAGCA
Mdga2	95	300863062c3	F: CATTGCTTCAGTAAGGAACGTGT R: CCAAGAGCTTAATTGACGGAGAA
Myo1D	87	118026910c2	F: TGGGAGGGACACTGTCGAG R: TTGTAAGCAGCGTCAGCAATA
Thrsp	63	31560631c1	F: ATGCAAGTGCTAACGAAACGC R: GGAGTACCGATCCATGACTGTC
Hic1	97	148228528c3	F: ACTCCAGACCCGTTTCGAG R: CGTGCTTCATCCAGCGGTA
Wnt5a	77	371940978c1	F: CAACTGGCAGGACTTTCTCAA R: CCTTCTCCAATGTACTGCATGTG
Ufsp2	83	20149753c2	F: TTGACGCCGTTGTGTCTGTT R: TAGCTGCCTGAGAATTGCATC
Dot1L	112	40556380c1	F: GAGGCTCAAGTCGCCTGT R: GACCCACCGGATAGTCTCAAT
P2rx5	75	238624117c1	F: GCTCACCATCCTGTTGTACTTAC R: AGGGAAGTGTCAATGTCCTGA
Nxn	102	162287186c2	F: GGCTCCTGGTGATCCGAGAT R: GCCCGTTATTTCTAAGCAAGGG
Psat1	90	329299027c2	F: AAGGAGTGCTGACTACGTGGT R: GGGTGGACAATGTTCACGTT
Aldh3a1	80	163310770c3	F: TCCAGCGGGTCATAAATCTGA R: AGCTATGTATCGTGAAGGCTGAT

Normalization and Comparison of Relative Gene Expression:

qPCR data for each gene was normalized to compare relative expression levels between chondroclasts and osteoclasts via quantitative ΔΔCt analysis. The mean Ct values of the collective endogenous controls were used for internal normalization. Mean relative fold induction was calculated using the Comparative CT Method (ΔΔCt Method) from Applied Biosystems (21). For each sample, the mean Ct for each test gene was subtracted from the mean Ct value for the endogenous control (β-Actin). This gave the ΔCt for each sample and gene. The standard error was then calculated as the square root of the sum of the square of the standard deviation divided by the square root of the number of samples. The ΔΔCt was calculated by subtracting the ΔCt of the osteoclast from the ΔCt of the chondroclast. Finally, the relative fold change was calculated as $2^{-\Delta\Delta Ct}$ for each gene. The error bars were calculated as +/- the standard error for the ΔΔCt and calculated as $2^{-\Delta\Delta Ct+SE}$ and $2^{-\Delta\Delta Ct-SE}$.

RESULTS

TRAP Staining to Identify Chondroclasts and Osteoclasts on Histological Sections of E18.5 Mouse Embryos

E18.5 embryos were sectioned, deparaffinized and stained for TRAP. TRAP stain was left on each section for 12-20 minutes until TRAP-positive cells became identifiable under the microscope. The sections were then counterstained with Alcian Blue, which stains the cartilage. This was done in order to make it easier to distinguish between chondroclasts and osteoclasts based proximity to cartilage and bone, respectively. **Figure 1** shows a section from an E18.5 femur that has been stained for TRAP and counterstained with Alcian Blue. As shown in this figure, chondroclasts were located on or near hypertrophic chondrocytes and osteoclasts were located on mineralized bone. There were a number of TRAP-positive cells that were not associated with either cartilage or bone. These were not captured as it was unclear whether these would be chondroclasts or osteoclasts.

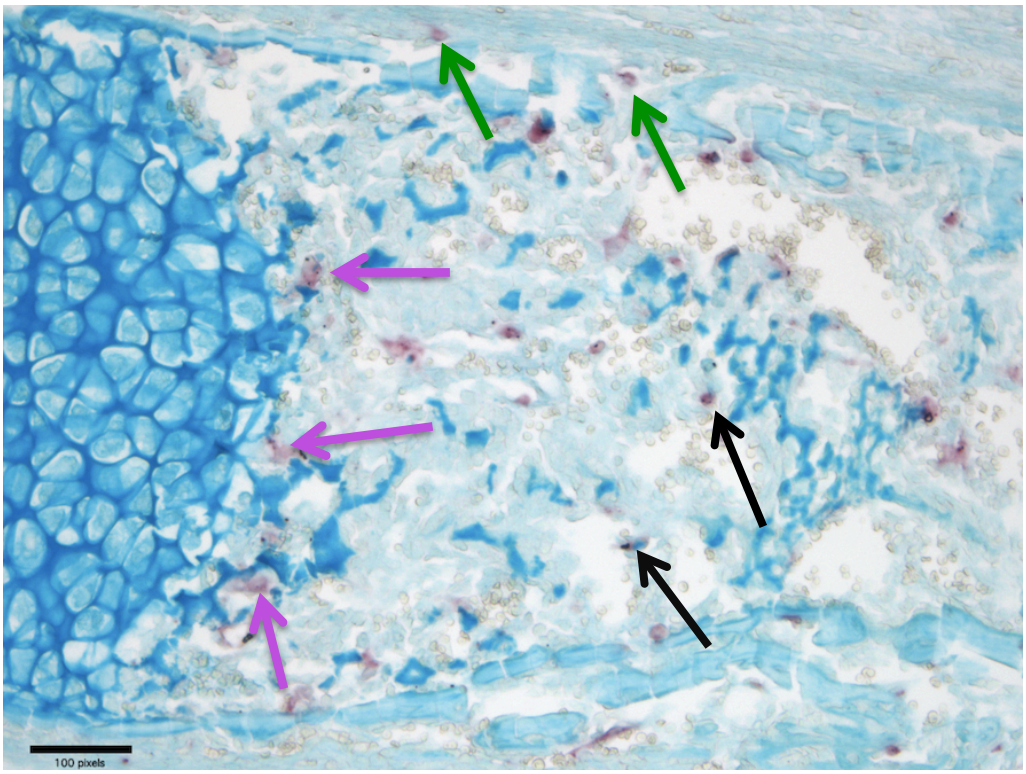

Figure 1: 200X photograph of a TRAP stained section from an E18.5 femur, counterstained with Alcian Blue (which stains cartilage). Pink arrows denote TRAP-positive (red-stained) chondroclasts sitting on and around hypertrophic cartilage. Green arrows denote TRAP-positive (red-stained) osteoclasts sitting on the bone and away from the bone marrow cavity. Black arrows denote TRAP-positive cells that were neither adjacent to the hypertrophic cartilage nor adjacent to bone that were not collected.

LCM to Capture Homogenous Population of Chondroclasts and Osteoclasts

Once TRAP-positive chondroclasts and osteoclasts had been located, the cells were captured using LCM. This technology allows for the isolation of individual cells, directly from the sample without pulling up too much unwanted material from the region around the desired cell. LCM facilitates capture of homogenous populations of cells. **Figure 2** illustrates the LCM microscope that was used to captured and collect cells. **Figure 3** depicts the before, during and after the capture of a cell. For chondroclasts and osteoclasts, I captured 10-20 individual cells (chondroclasts or osteoclasts) on each cap and stored the caps at -20 degrees Celsius prior to RNA lysis.

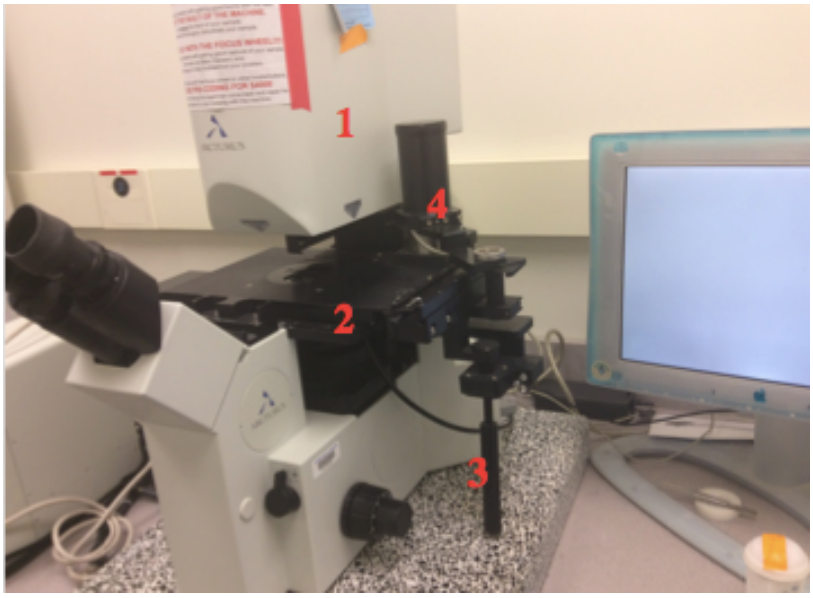

Figure 2: Main components of laser capture microdissection and how it is performed. **1.** Laser Housing **2.** Dock for slide **3.** Joystick to move dock **4.** Arm to hold, pick up and move the LCM cap.

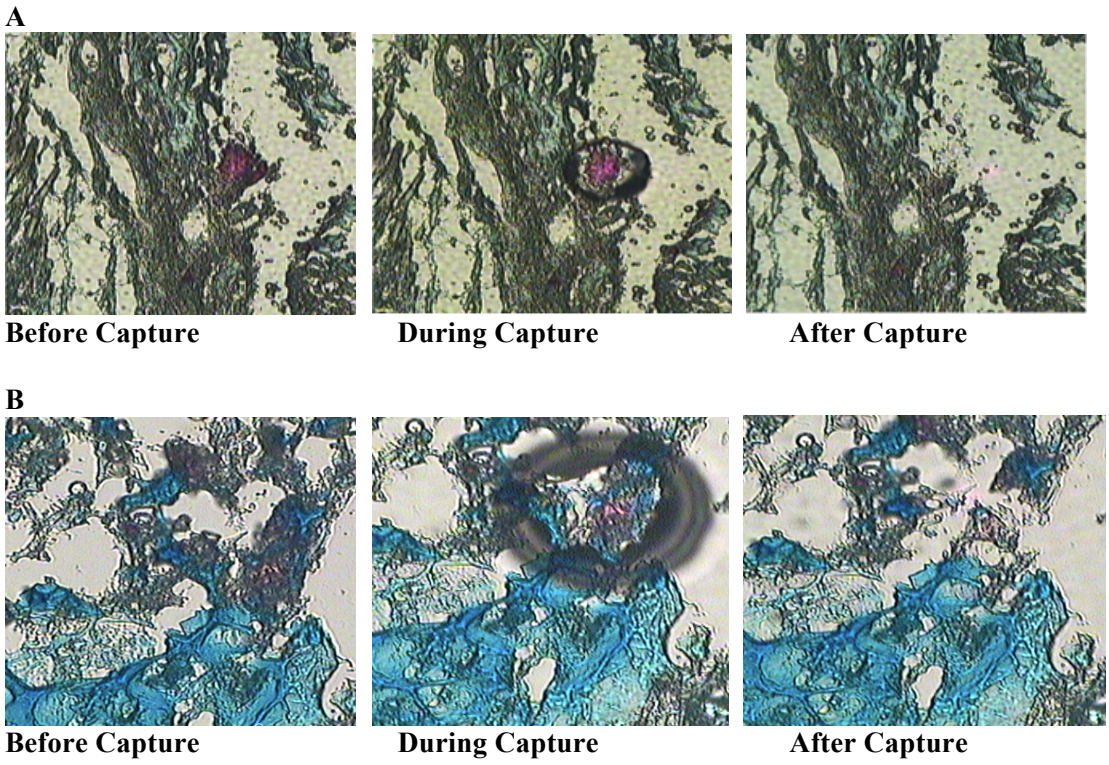

Figure 3: (A) LCM showing before, during and after capture of a TRAP positive osteoclast (B) LCM illustrating before, during and after capture of a TRAP-positive chondroclast. In both A and B, note the ring of melted polymer surrounding the cell to be captured. In the after capture, the TRAP-positive cell has been removed.

RT-qPCR for Endogenous Controls and Known Markers for Osteoblast and Hypertrophic Chondrocyte Expression

The first step of the project was to isolate, amplify, and assess levels of genes that were ubiquitously expressed in all cells of the mouse, in order to test the quality of the RNA that had been collected from the TRAP-positive cells. To do this, I chose three genes as my endogenous controls; glyceraldehyde 3-phosphate dehydrogenase (Gapdh), β-Actin (Actb) and Ubiquitin C (Ubc) (**Table 2**). In addition to my endogenous controls, I also performed qPCR for two markers known to be specific for osteoblast and hypertrophic chondrocyte cells (**Table 3**) (22, 23), in order to rule out contamination of the samples that I collected.

RT-qPCR analysis allows relative quantitation of RNA levels present in the cells. The relative quantitation relies on the determination of the cycle threshold. The cycle threshold is the number of rounds of PCR amplification (cycles) necessary for the fluorescent signal created by incorporation of fluorescent labeled nucleotides into the PCR product to cross a predetermined threshold. The lower the Ct number, the higher the concentration of RNA in the sample.

After running qPCR for the endogenous controls and analyzing the cycle threshold (Ct) values, I found that the Ct values for the endogenous genes were between 15 and 23 (**Figure 3**). These values showed that my RNA samples had been successfully amplified. This was important because all of the steps required to collect the RNA were heavily damaging to the RNA, yet I was successful in obtaining usable RNA for my analyses.

The other critical question in this initial qPCR test was the potential level of contamination of the TRAP-positive cells by chondrocytes and osteoblasts. After running the qPCR, I analyzed the Ct values for Sp7, an osteoblast marker gene, and Col10A1, a chondrocyte marker gene. I saw that the Ct values for Sp7 were greater than 30 (**Figure 4**). Ct values greater than 30 suggest that very little Sp7 RNA in the samples. This suggests that there was little osteoblast contamination in the clastic cell samples that I collected. However, for my Col10A1 analysis, which is a marker for hypertrophic chondrocytes, the Ct value fell below the Ct 30

threshold, raising concerns regarding contamination. To further rule out contamination, I isolated hypertrophic chondrocytes by LCM, extracted RNA from cells and compared levels of expression of Col10A1 from the chondrocytes to the level of expression in my chondroclast samples. Comparing expression between the chondrocyte and chondroclast, I saw that there was a 230-fold increased expression of Col10A1 in the chondrocyte samples relative to the chondroclast samples (**Table 4**). This suggested that there was minimal contamination of my chondroclast samples by hypertrophic chondrocytes. Having ruled out contamination and chosen to use β-Actin as my endogenous control, I was now able to run my qPCR for my candidate genes.

Genes	Full name/Protein	Function
Gapdh	Glyceraldehyde 3-phosphate dehydrogenase	Involved in transcription, RNA transport, DNA replication and apoptosis
Actb	Beta-Actin	Involved in cell motility and are ubiquitously expressed in all eukaryotic cells
Ubc	Ubiquitin C	Associated with protein degradation, DNA repair, cell cycle regulation, kinase modification, endocytosis, and regulation of other cell signaling pathways

Table 2: Potential Endogenous Control Genes

Genes Gapdh, B-Actin and Ubc are the endogenous control genes that are ubiquitously expressed in the cells of mouse.

Genes	Full name/Protein	Function
Col10A1	Collagen, Type X, Alpha 1	Short chain collagen expressed by hypertrophic chondrocytes during endochondral ossification
Sp7	Zinc Finger Protein Osterix	Bone specific transcription factor required for osteoblast differentiation and bone formation

Table 3: Known Markers of Chondrocyte and Osteoblast Cells

Genes Col10A1 and Sp7/Osterix, are known markers for hypertrophic cartilage and osteoblast, respectively (22, 23)

[1]

[1] Gene information was obtained from GeneCards®: The Human Gene Database

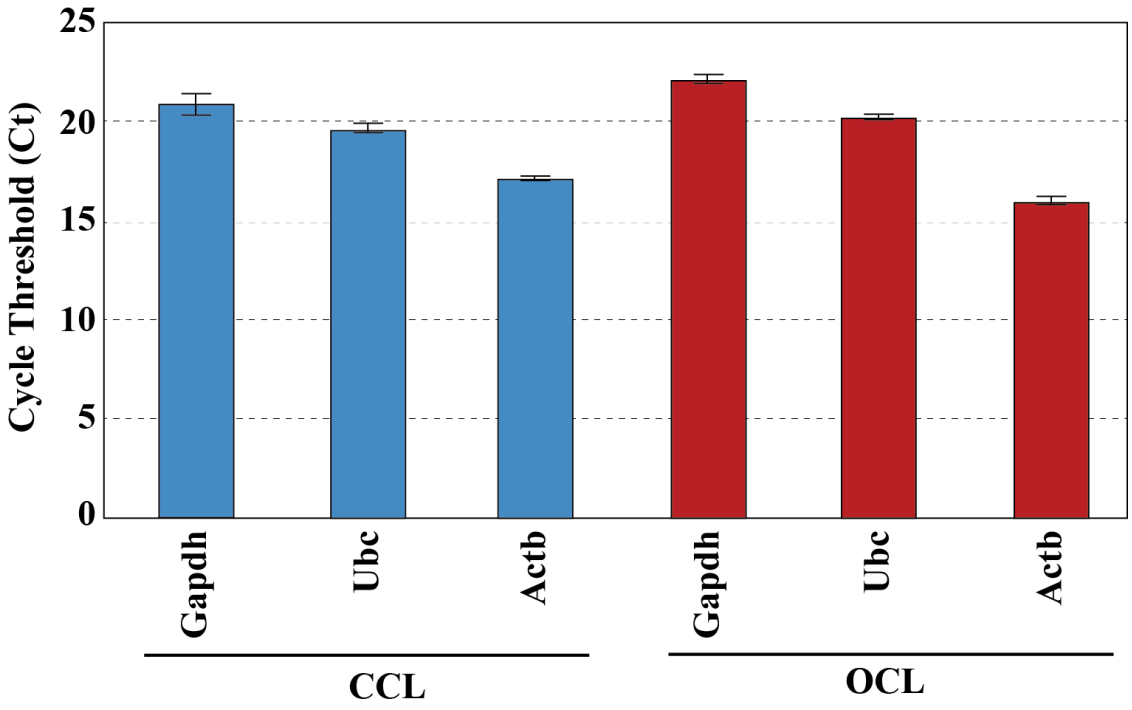

Figure 4: Expression of three different housekeeping genes in RNA from LCM-captured chondroclast and osteoclast samples. Ct values represent the number of qPCR cycles it takes for a signal to be detected. The lower the Ct value, the more RNA of that gene in the sample. Ct values of 15-23 suggest good yields of RNA in the samples.

CCL – chondroclast; OCL - osteoclast

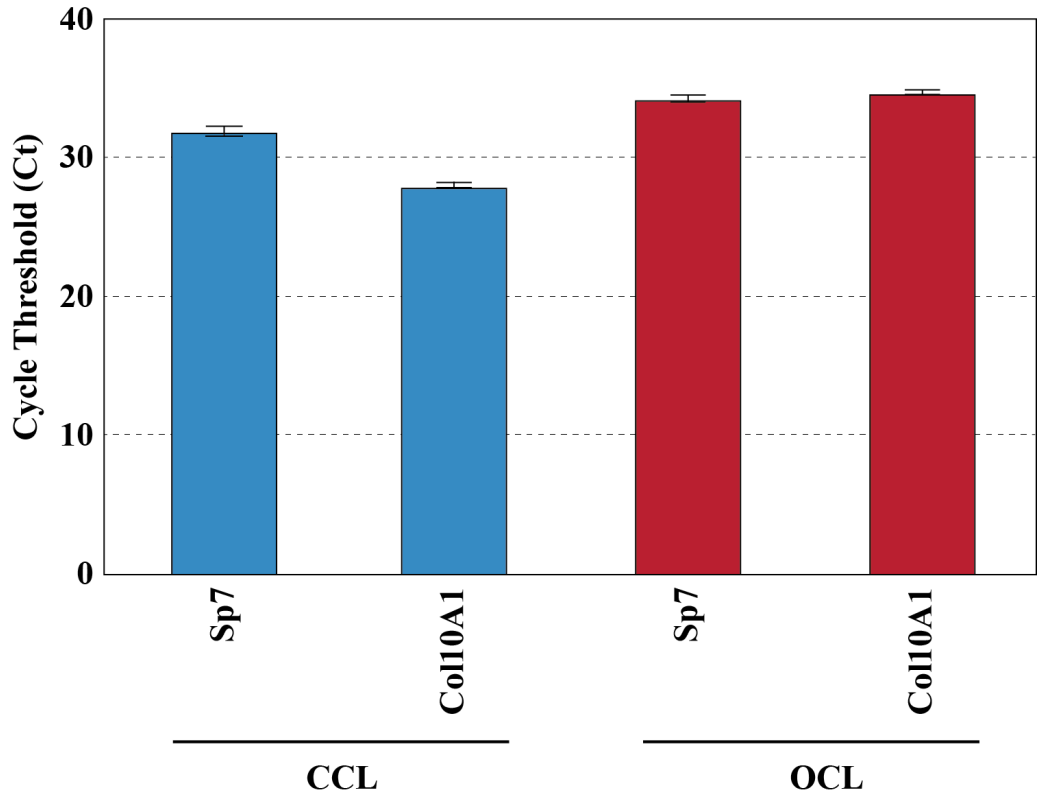

Figure 5: Expression of known markers for osteoblasts and hypertrophic chondrocytes. Sp7 expression in chondroclasts and osteoclasts had Ct values >30, while Ct values for the endogenous controls (Actb) were ≤17 (Figure 3), which suggested very low to no expression of Sp7 in the chondroclast/osteoclast samples, consistent with very low to no contamination of osteoblasts in either LCM-captured sample. Ct values for Col10A1 expression in the osteoclast samples were also in excess of 30, which suggested low to no contamination of hypertrophic chondrocytes in the LCM-captured osteoclast samples. However, Ct values for Col10A1 in the chondroclast samples were in the 27-28 range, which required additional analysis to determine whether this expression was consistent with a possible significant level of contaminating chondrocytes.

CCL – chondroclast; OCL - osteoclast

	COL10A1	B-Actin	ΔCt	ΔΔCt	Fold Expression
CCL	28.003	17.19	10.81	7.85	230
HC	28.816	25.84	2.98		

Table 4: Relative quantitation of Col10A1 expression in chondroclasts and hypertrophic chondrocytes. Quantitative comparison of expression using the ΔΔCt method was done to determine the possible levels of contamination of chondrocytes in the chondroclast samples. There was a 230-fold greater level of expression of Col10A1 in the RNA from the hypertrophic chondrocytes than in the chondroclasts when normalized to Actb expression suggesting that there was little to no expression of Col10A1 in the CCL samples and thus the data were consistent with little to no contamination of the CCL samples by chondrocytes.

CCL – chondroclast; HC – hypertrophic chondrocyte

RT-qPCR Analysis Using a Candidate Gene Approach

The thirteen candidate genes selected for my analysis were chosen from among those that had been found to be differentially expressed between chondroclasts and osteoclasts in a mouse fracture model (**Table 5**). I wanted to test whether these genes were differentially expressed between chondroclasts and osteoclasts in the developing mouse. Each gene was tested in each of three independent LCM-captured samples of chondroclasts and osteoclasts. qPCR analysis of the RNA from the chondroclasts and osteoclasts samples for the selected genes revealed Ct values between 18 and 32 **(Figure 5).**

Genes	Full name/Protein	Function
Zfp595	Zinc finger protein 595	DNA template-transcription
Aldh3a1	Aldehyde Dehydrogenase 3 Family, Member A1	Detoxification of alcohol-derived acetaldehydes; involved in metabolism of corticosteroids, biogenic amines, neurotransmitters and lipid peroxidation
Psmb9/Lmp2	Proteasome Subunit Beta 9	Cleaves peptides in an ATP/ubiquitin-dependent process; the modified proteasome processes class I MHC peptides
Thrsp	Thyroid hormone-inducible hepatic protein	Regulation of lipogenesis (lactating mammary glands)
Hic1	Hypermethylated in cancer 1 protein	Growth regulatory and tumor suppressor
Mdga2	MAM domain containing glycosylphosphatidylinositol anchor 2	Required for radial migration of cortical neurons; maintenance of inhibitory synapses
Dot1L	DOT1-like, histone H3 methyltransferase (*S. cerevisiae*)	Histone methyltransferase that methylates lysine-79 of histone H3
P2rx5	Purinergic Receptor P2X, Ligand Gated Ion Channel, 5	Ligand-gated ion channel. Alternative splicing results in multiple transcripts
Nxn	Nucleoredoxin	Redox-dependent regulator of the Wnt signaling pathway; involved in cell growth and differentiation
Ufsp2	UFM1-Specific Peptidase 2	A thiol protease that processes the C terminus of ubiquitin-fold modifier 1 (UFM1)
Wnt5a	Wingless-Type MMTV Integration Site Family, Member 5A	Involved in oncogenesis and developmental processes (regulation of cell fate and patterning during embryogenesis)
Myo1D	Myosin ID	Actin –based motor molecules with ATPase activity
Higd2A	HIG1 Hypoxia Inducible Domain Family, Member 2A	Contains a subunit of cytochrome c oxidase that catalyzes the reduction of oxygen to water

Table 5: Candidate Genes. Genes shown here were some of the most differentially expressed genes between OCL and CCL in the fracture mouse model.

[2]

[2] Gene information was obtained from GeneCards®: The Human Gene Database

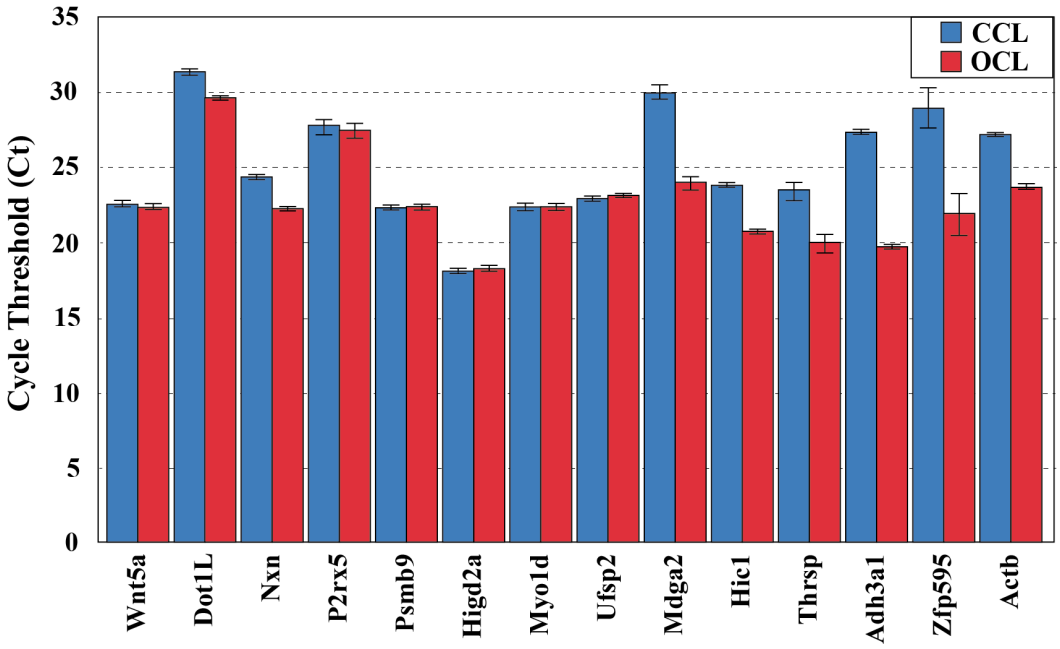

Figure 6: Ct values for candidate genes in chondroclasts and osteoclasts in the E18.5 embryo. The efficiency of the amplification of each gene is relatively equal to that of the amplification of the endogenous control (*Actb*).

CCL – chondroclasts; OCL - osteoclasts

Relative Quantitation of Gene Expression by ΔΔCt Method:

The ΔΔCt method of relative quantitation can be used to compare differences in relative levels of expression of genes (21). We used this method to compare levels of gene expression between chondroclasts and osteoclasts for thirteen genes. To do this, ΔCt values were obtained by subtracting the mean Ct values of the endogenous control gene (*Actb*) from the experimental gene. This analysis is considered best used when the Ct values for the endogenous control are similar to values of the experimental gene. ΔΔCt values are obtained by subtracting the mean osteoclast ΔCt value from the mean chondroclast ΔCt value. The log ΔΔCt values of all thirteen genes tested are shown in **Figure 6**. Negative values correspond to increased relative expression in chondroclasts while positive values correspond to increased relative expression in osteoclasts. I then calculated the relative fold difference of expression between the chondroclasts and osteoclasts using the formula $RF = 2^{-\Delta\Delta Ct}$. The results are plotted in **Figure 7**. Together, these data indicate that the gene expression profile of osteoclasts and chondroclasts is different.

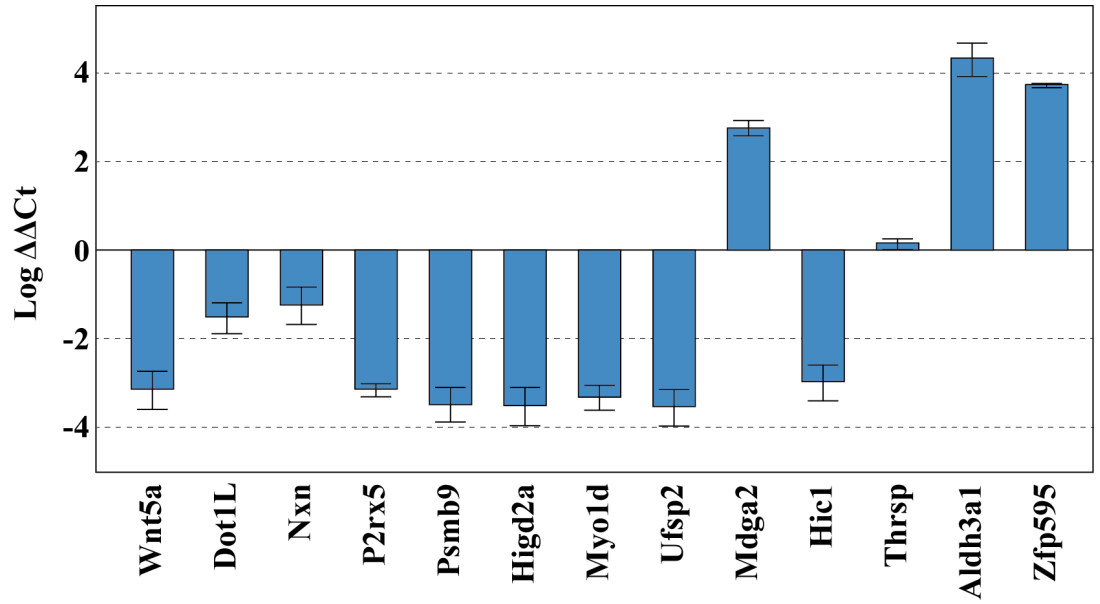

Figure 7: Log fold expression ratio for E18.5, calculated using Comparative ΔΔCt Method (citation needed). Negative ΔΔCt values mean that the gene is more highly expressed in chondroclasts. Positive ΔΔCt values mean that the gene is more highly expressed in osteoclasts.

CCL – chondroclast; OCL - osteoclast

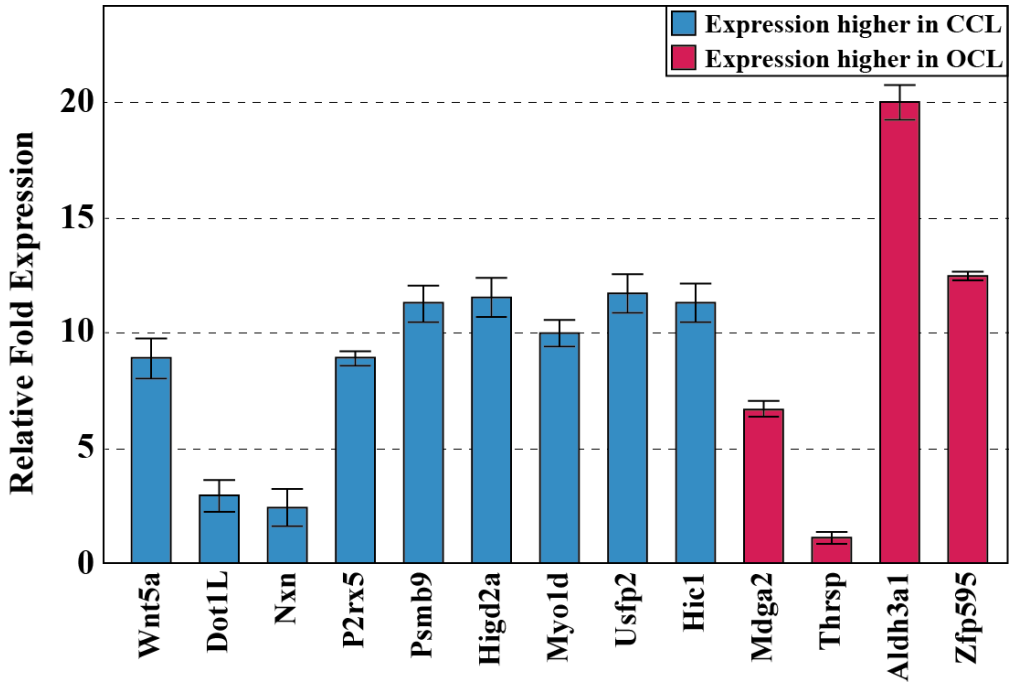

Figure 8: Mean relative fold induction for chondroclasts and osteoclasts in the E18.5 embryo. Relative fold induction is calculated as: $RF=2^{-\Delta\Delta Ct}$

CCL – chondroclasts; OCL - osteoclasts

DISCUSSION

Remodeling of mineralized cartilage is an essential step in the process of endochondral ossification that occurs during development **(Figure 9).** The term chondroclast has been assigned to the multi-nucleated TRAP-positive cells found near hypertrophic cartilage, with the unique function of remodeling mineralized cartilage matrix. While it is generally believed that both osteoclasts and chondroclasts arise from the same monocyte/macrophage precursor, it is not known what causes these two clastic cells to differentiate into two different cell types. However, it is likely that the signal to differentiate into the two different clastic cells comes from the unique microenvironments into which these two cells invade.

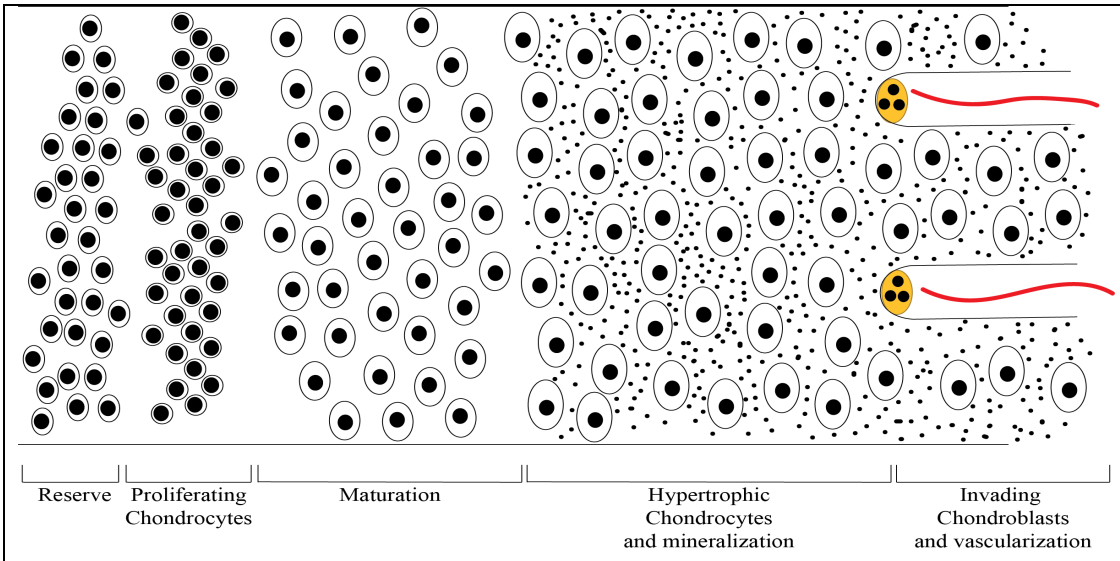

Figure 9. Critical role for chondroclasts in remodeling mineralized cartilage during endochondral ossification. The chondroclasts provide routes for the vascularization of the mineralized hypertrophic chondrocytes that in turn will allow invasion of osteoblasts and subsequent ossification (24).

While the genes necessary for osteoclastogenesis have been widely characterized (25) little is known about the genetic similarities or differences between osteoclasts and chondroclasts.

Therefore, my research sought to explore the genomic expression profile of these two similar cells in a developmental model.

Key to the success of my project was the ability to collect homogeneous populations of TRAP-positive cells adjacent to either the hypertrophic chondrocytes or the mineralizing bone. Laser capture microdissection enabled me to individually select cells and to capture them for subsequent analysis. After successfully capturing the TRAP-positive chondroclastic and osteoclastic cells, the ability to isolate and linearly amplify RNA from the small number of cells that I captured was another key to the success of this project. The RNA isolation and amplification protocol developed by Gibson *et al* (20), as modified by the Drissi laboratory, was critical for my ability to obtain sufficient amplified cDNA to enable me to run the qPCR to analyze the candidate genes. What I found was that there are clear differences between chondroclasts and osteoclasts in the expression profiles of the candidate genes I chose. These results supported and validated the hypothesis that chondroclasts and osteoclasts have different genomic profiles during embryonic development at time point E18.5.

The candidate genes that I chose to examine had come from the set of differentially expressed genes that had been identified in the TRAP-positive cells within the healing mouse bone fracture (18). The genes that were observed in this study were chosen based on a variety of classifications. These include genes were involved in binding [Zfp595, P2rx5, Myo1D and Wnt5a], catalytic activity (Nxn, Dot1L, Aldh3a1 and Myo1D), enzyme regulator activity (Myo1D), transcription factor activity (Zfp595), receptor activity (P2rx5), a structural molecule (Myo1D) and transporter activity (P2rx5) (**Table 6).** In addition to similar classifications, these genes are co-expressed together and also have genetic interactions. P2rx5, Myo1D and Higd2a are known to be co-expressed together (26, 27) while Nxn and Wnt5a are also known to be co-expressed together (27, 28). Higd2a and Thrsp have a known genetic interaction (29). The interaction maps in **Figure 10**, illustrate the broad range of interaction that these genes have. For instance, Hic1 indirectly interacts with Pax1, which directly interacts with Myo1D (**Figure 10C**).

It is through these classifications and interactions that we may come to understand what is happening in the microenvironment of these two clastic cells.

When looking at the differences in expression of these genes between chondroclasts and osteoclasts, is important to note the microenvironments in which both cell types are found. To explain this, we have created a working model in order to demonstrate the kinds of interactions that are taking place in the microenvironments of these two cell types (**Figure 11**). This model illustrates the lineage of chondroclasts and osteoclasts; both cell types arise from a hematopoietic stem cell, which is differentiated into a monocyte/macrophage precursor cell. These precursor cells, which are circulating in the blood stream, differentiate into pre-osteoclasts when stimulated by macrophage colony stimulating factor (M-CSF) (30). This pre-osteoclast further differentiates into an active osteoclast when stimulated by RANKL, giving rise to a cell that can now adhere to the bone and begin resorption (31). However, what is not known is what causes the monocyte/macrophage precursor cell to differentiate into the chondroclast. It is possible that M-CSF and RANKL may also be involved in the differentiation of the chondroclast, but there could also be some other transcription factor, integrin or soluble factor that is responsible for the chondroclast lineage.

In the future, we hope to examine more candidate genes and begin to build a genomic signature so that we can use this genomic signature to identify distinct signaling pathways that may regulate the two types of clastic cells. We would also like to look at additional time points (E15.5, E16.5 and post-natal), to examine whether changes in genetic expression of chondroclasts and osteoclasts vary temporally. It is important to do this because the expression of genes at an earlier time point may be different from that of a later time point, particularly since the microenvironment in which these cells are found change as endochondral ossification progresses. Lastly, we would like to interrogate the functionality of these genomic changes in both *in vitro* and *in vivo* models. In one such example, my laboratory has developed a conditional knockout mouse model for the gene, Dot1L. Since Dot1L plays a role in embryonic development and

hematopoiesis, knocking it out in chondroclasts and osteoclasts would tell us if and what type of skeletal phenotype the mouse may have. It will also tell us how severe the skeletal phenotype is; given that it is up-regulated in chondroclasts in the developmental model. It is critical to understand what is happening at this point as this will tell us why the two cell types are different.

Understanding how the differential gene expression in these two cell types may play a role in a fracture repair model, for instance, could tell us whether knocking out one of these factors would improve or delay fracture healing. In the same way, we can examine whether these cells play a role in the other disease models, such as osteoarthritis or rheumatoid arthritis. As an example, Knowles et al conducted a study on rheumatoid arthritis using mature human clastic cells and observed what they termed chondroclasts on the deep surface of resorbed hyaline cartilage in this disease (15). Chondroclasts are predominantly found during the early stages endochondral ossification, so that by the time the bone is fully developed, there is very little to no trace of chondroclasts. In addition to this, chondroclasts are normally found on or near hypertrophic cartilage, rather than on the deep hyaline cartilage. It is possible that examining the genetic profile of chondroclasts that are found in the rheumatoid joint will help discover what genes are involved in signaling these chondroclasts to aberrantly appear in the sites of subchondral erosion. It is also possible that developing conditional knockout mouse models of these genes will lead to understanding how to prevent the breakdown of cartilage in rheumatoid arthritis.

Thus, identifying and testing the functional differences in the genomic profile of osteoclasts and chondroclasts will be instrumental in developing new strategies to target these cells in diseases such as osteoarthritis, osteoporosis, rheumatoid arthritis and fracture.

Dot1L	DOT1-like, histone H3 methyltransferase (S. cerevisiae)
GOTERM_MF_FAT	DNA binding, N-methyltransferase activity, protein methyltransferase activity, lysine N-methyltransferase activity, protein-lysine N-methyltransferase activity, histone-lysine N-methyltransferase activity, histone methyltransferase activity,
INTERPRO	Histone methylation DOT1, AT hook, DNA-binding, conserved site,
KEGG_PATHWAY	Lysine degradation,
PIR_SUPERFAMILY	PIRSF037123:histone H3-K79 methyltransferase, animal type,
SMART	AT_hook,
SP_PIR_KEYWORDS	methyltransferase, transferase,
Higd2A	**HIG1 domain family, member 2A**
GOTERM_CC_FAT	mitochondrion, integral to membrane, intrinsic to membrane,
INTERPRO	Hypoxia induced protein conserved region,
SP_PIR_KEYWORDS	acetylation, membrane, transmembrane,
UP_SEQ_FEATURE	chain:HIG1 domain family member 2A, domain:HIG1, modified residue, topological domain:Cytoplasmic, topological domain:Extracellular, transmembrane region,
Mdga2	**MAM domain containing glycosylphosphatidylinositol anchor 2**
GOTERM_BP_FAT	spinal cord development, cell differentiation in spinal cord, ventral spinal cord development, spinal cord motor neuron differentiation, neuron differentiation,
GOTERM_CC_FAT	plasma membrane, intrinsic to membrane, anchored to membrane,
INTERPRO	MAM, Immunoglobulin subtype 2, Immunoglobulin subtype, Immunoglobulin-like, Immunoglobulin I-set, Immunoglobulin, Immunoglobulin-like fold,
SMART	MAM, IGc2, IG,
SP_PIR_KEYWORDS	cell membrane, disulfide bond, glycoprotein, gpi-anchor, Immunoglobulin domain, lipoprotein, membrane, repeat, signal,
UP_SEQ_FEATURE	chain:MAM domain-containing glycosylphosphatidylinositol anchor protein 2, disulfide bond, domain:Ig-like 1, domain:Ig-like 2, domain:Ig-like 3, domain:Ig-like 4, domain:Ig-like 5, domain:Ig-like 6, domain:MAM, glycosylation site:N-linked (GlcNAc...), lipid moiety-binding region:GPI-anchor amidated aspartate, propeptide:Removed in mature form, signal peptide,
Ufsp2	**UFM1-specific peptidase 2**
GOTERM_BP_FAT	proteolysis, macromolecule catabolic process, modification-dependent protein catabolic process, protein catabolic process, modification-dependent macromolecule catabolic process, cellular protein catabolic process, cellular macromolecule catabolic process, proteolysis involved in cellular protein catabolic process,
GOTERM_MF_FAT	peptidase activity, cysteine-type peptidase activity, thiolester hydrolase activity, peptidase activity, acting on L-amino acid peptides,
INTERPRO	Peptidase C78, ubiquitin fold modifier-specific peptidase 1 and 2,
SP_PIR_KEYWORDS	hydrolase, Protease, thiol protease, ubl conjugation pathway,
UP_SEQ_FEATURE	chain:Ufm1-specific protease 2, mutagenesis site,
Aldh3a1	**aldehyde dehydrogenase family 3, subfamily A1**
GOTERM_BP_FAT	cellular aldehyde metabolic process, oxidation reduction,
GOTERM_CC_FAT	cytosol,
GOTERM_MF_FAT	3-chloroallyl aldehyde dehydrogenase activity, aldehyde dehydrogenase (NAD) activity, aldehyde dehydrogenase [NAD(P)+] activity, aldo-keto reductase activity, alcohol dehydrogenase (NADP+) activity, oxidoreductase activity, acting on the aldehyde or oxo group of donors, NAD or NADP as acceptor,
INTERPRO	Aldehyde dehydrogenase NAD(P)-dependent, Aldehyde dehydrogenase, Aldehyde dehydrogenase, conserved site, Aldehyde dehydrogenase, N-terminal,
KEGG_PATHWAY	Glycolysis / Gluconeogenesis, Histidine metabolism, Tyrosine metabolism, Phenylalanine metabolism, Metabolism of xenobiotics by cytochrome P450, Drug metabolism,
PIR_SUPERFAMILY	PIRSF036492:aldehyde dehydrogenase, PIRSF036492:ALDH,
SP_PIR_KEYWORDS	acetylation, cytoplasm, nadp, oxidoreductase, polymorphism,
UP_SEQ_FEATURE	chain:Aldehyde dehydrogenase, dimeric NADP- preferring, modified residue, nucleotide phosphate-binding region:NAD, sequence variant,
Hic1	**hypermethylated in cancer 1**
COG_ONTOLOGY	General function prediction only,
GOTERM_BP_FAT	transcription, regulation of transcription,
GOTERM_MF_FAT	DNA binding, zinc ion binding, ion binding, cation binding, metal ion binding, transition metal ion binding,
INTERPRO	BTB/POZ-like, Zinc finger, C2H2-type, BTB/POZ fold, BTB/POZ, Zinc finger, C2H2-type/integrase, DNA-binding, Zinc finger, C2H2-like,
SMART	BTB, ZnF_C2H2,
SP_PIR_KEYWORDS	acetylation, alternative splicing, developmental protein, dna-binding, isopeptide bond, metal-binding, nucleus, phosphoprotein, repeat, Transcription, transcription regulation, ubl conjugation, zinc, zinc-finger,
UP_SEQ_FEATURE	chain:Hypermethylated in cancer 1 protein, compositionally biased region:Arg/Gly/Pro-rich, compositionally biased region:Poly-Ala, compositionally biased region:Poly-Gly, compositionally biased region:Poly-Pro, cross-link:Glycyl lysine isopeptide (Lys-Gly) (interchain with G-Cter in SUMO); alternate, domain:BTB, modified residue, region of interest:Binding to CtBP, sequence conflict, zinc finger region:C2H2-type 1, zinc finger region:C2H2-type 2, zinc finger region:C2H2-type 3, zinc finger region:C2H2-type 4, zinc finger region:C2H2-type 5,

Myo1D	myosin ID
GOTERM_CC_FAT	cytoskeleton, actin cytoskeleton, myosin complex, non-membrane-bounded organelle, intracellular non-membrane-bounded organelle, cytoskeletal part,
GOTERM_MF_FAT	nucleotide binding, nucleoside binding, purine nucleoside binding, motor activity, actin binding, calmodulin binding, ATP binding, cytoskeletal protein binding, purine nucleotide binding, adenyl nucleotide binding, ribonucleotide binding, purine ribonucleotide binding, adenyl ribonucleotide binding,
INTERPRO	IQ calmodulin-binding region, Myosin head, motor region, Myosin tail 2,
SMART	IQ, MYSc,
SP_PIR_KEYWORDS	acetylation, actin-binding, alternative splicing, atp-binding, calmodulin-binding, motor protein, myosin, nucleotide-binding, phosphoprotein, repeat,
UP_SEQ_FEATURE	chain:Myosin-Id, domain:IQ 1, domain:IQ 2, domain:Myosin head-like, modified residue, nucleotide phosphate-binding region:ATP, splice variant,
Nxn	**nucleoredoxin**
GOTERM_BP_FAT	cell surface receptor linked signal transduction, Wnt receptor signaling pathway, cellular homeostasis, homeostatic process, cell redox homeostasis, oxidation reduction,
GOTERM_CC_FAT	cytosol,
GOTERM_MF_FAT	thioredoxin-disulfide reductase activity, antioxidant activity, oxidoreductase activity, acting on NADH or NADPH, oxidoreductase activity, acting on sulfur group of donors, oxidoreductase activity, acting on sulfur group of donors, NAD or NADP as acceptor, protein-disulfide reductase activity,
INTERPRO	Alkyl hydroperoxide reductase/ Thiol specific antioxidant/ Mal allergen, Thioredoxin fold, Thioredoxin-like, Thioredoxin, conserved site,
SP_PIR_KEYWORDS	alternative splicing, cytoplasm, developmental protein, differentiation, nad, nucleus, oxidoreductase, wnt signaling pathway,
UP_SEQ_FEATURE	chain:Nucleoredoxin, domain:Thioredoxin, mutagenesis site, splice variant,
Psmb9	**proteasome (prosome, macropain) subunit, beta type 9 (large multifunctional peptidase 2)**
GOTERM_BP_FAT	proteolysis, immune response, macromolecule catabolic process, antigen processing and presentation, protein catabolic process, cellular protein catabolic process, cellular macromolecule catabolic process, proteolysis involved in cellular protein catabolic process,
GOTERM_CC_FAT	proteasome complex, endoplasmic reticulum, cytosol, proteasome core complex, MHC class I peptide loading complex, TAP complex, endoplasmic reticulum part,
GOTERM_MF_FAT	nucleotide binding, nucleoside binding, purine nucleoside binding, endopeptidase activity, threonine-type endopeptidase activity, ATP binding, peptidase activity, purine nucleotide binding, adenyl nucleotide binding, ribonucleotide binding, purine ribonucleotide binding, adenyl ribonucleotide binding, peptide binding, MHC protein binding, MHC class I protein binding, threonine-type peptidase activity, peptidase activity, acting on L-amino acid peptides,
INTERPRO	Peptidase T1A, proteasome beta-subunit, Proteasome, alpha and beta subunits, Proteasome, subunit alpha/beta, Proteasome, beta-type subunit, conserved site,
KEGG_PATHWAY	Proteasome,
PIR_SUPERFAMILY	PIRSF001214:multicatalytic endopeptidase complex chain C5,
SP_PIR_KEYWORDS	acetylation, cytoplasm, cytosol, hydrolase, immune response, nucleus, polymorphism, Protease, proteasome, threonine protease, zymogen,
UP_SEQ_FEATURE	active site:Nucleophile, chain:Proteasome subunit beta type-9, modified residue, propeptide:Removed in mature form, sequence variant, site:Cleavage; by autocatalysis,
P2rx5	**purinergic receptor P2X, ligand-gated ion channel, 5**
GOTERM_BP_FAT	ion transport, cell surface receptor linked signal transduction,
GOTERM_CC_FAT	plasma membrane, integral to plasma membrane, integral to membrane, intrinsic to membrane, intrinsic to plasma membrane, plasma membrane part,
GOTERM_MF_FAT	nucleotide binding, nucleoside binding, purine nucleoside binding, ATP-gated cation channel activity, ion channel activity, extracellular ligand-gated ion channel activity, cation channel activity, ATP binding, channel activity, ligand-gated ion channel activity, purine nucleotide binding, passive transmembrane transporter activity, ligand-gated channel activity, gated channel activity, substrate specific channel activity, adenyl nucleotide binding, ribonucleotide binding, purine ribonucleotide binding, adenyl ribonucleotide binding, metal ion transmembrane transporter activity,
INTERPRO	P2X purinoreceptor, P2X5 purinoceptor,
KEGG_PATHWAY	Calcium signaling pathway, Neuroactive ligand-receptor interaction,
SP_PIR_KEYWORDS	ion transport, ionic channel, receptor, transmembrane, transport,
Thrsp	**thyroid hormone responsive SPOT14 homolog (Rattus)**
INTERPRO	Thyroid hormone-inducible hepatic Spot 14,
PIR_SUPERFAMILY	PIRSF023977:PIRSF023977,
SP_PIR_KEYWORDS	nucleus,
UP_SEQ_FEATURE	chain:Thyroid hormone-inducible hepatic protein,

Wnt5a	wingless-related MMTV integration site 5A
GOTERM_BP_FAT	MAPKKK cascade, skeletal system development, urogenital system development, morphogenesis of a branching structure, morphogenesis of an epithelium, reproductive developmental process, protein amino acid phosphorylation, phosphorus metabolic process, phosphate metabolic process, cell surface receptor linked signal transduction, Wnt receptor signaling pathway, calcium modulating pathway, intracellular signaling cascade, protein kinase cascade, JNK cascade, cell-cell signaling, ectodermal gut development, hindgut morphogenesis, sex differentiation, cell proliferation, negative regulation of cell proliferation, gonad development, male gonad development, Wnt receptor signaling pathway, phosphorylation, diencephalon development, pituitary gland development, gland morphogenesis, respiratory tube development, lung development, embryonic limb morphogenesis, mammary gland development, forebrain development, stress-activated protein kinase signaling pathway, cellular response to stress, mammary gland epithelial cell proliferation, appendage morphogenesis, limb morphogenesis, embryonic appendage morphogenesis, tube morphogenesis, endocrine system development, tube development, growth, regulation of cell proliferation, thelarche, development of secondary sexual characteristics, development of primary sexual characteristics, regulation of embryonic development, development of secondary female sexual characteristics, development of primary male sexual characteristics, female sex differentiation, male sex differentiation, digestive tract morphogenesis, gut morphogenesis, gut development, ectodermal gut morphogenesis, developmental growth, embryonic morphogenesis, reproductive structure development, tissue morphogenesis, gland development, appendage development, branching morphogenesis of a tube, hypophysis morphogenesis, diencephalon morphogenesis, forebrain morphogenesis, brain morphogenesis, epithelial cell proliferation, regulation of epithelial cell proliferation, negative regulation of epithelial cell proliferation, cartilage development, digestive system development, urinary bladder development, limb development, epithelium development, mammary gland morphogenesis, branching involved in mammary gland duct morphogenesis, respiratory system development, developmental growth involved in morphogenesis, epithelial tube morphogenesis, lateral sprouting involved in mammary gland duct morphogenesis, lateral sprouting from an epithelium, branch elongation of an epithelium, mammary gland duct morphogenesis, regulation of prostatic bud formation, negative regulation of prostatic bud formation, regulation of morphogenesis of a branching structure, mammary gland branching involved in thelarche, epithelial cell proliferation involved in mammary gland duct elongation, mammary gland duct branch elongation, regulation of branching involved in mammary gland duct morphogenesis,
GOTERM_CC_FAT	extracellular region, proteinaceous extracellular matrix, extracellular matrix, extracellular region part,
INTERPRO	Secreted growth factor Wnt protein, Secreted growth factor Wnt protein, conserved site,
KEGG_PATHWAY	Wnt signaling pathway, Hedgehog signaling pathway, Melanogenesis, Pathways in cancer, Basal cell carcinoma,
PIR_SUPERFAMILY	PIRSF001784:int-1 transforming protein,
SP_PIR_KEYWORDS	alternative splicing, Chondrogenesis, developmental protein, differentiation, direct protein sequencing, extracellular matrix, glycoprotein, lipoprotein, palmitate, Secreted, signal, wnt signaling pathway,
UP_SEQ_FEATURE	chain:Protein Wnt-5a, glycosylation site:N-linked (GlcNAc...), lipid moiety-binding region:S-palmitoyl cysteine, mutagenesis site, sequence conflict, signal peptide, splice variant,
Zfp595	**zinc finger protein 595**
COG_ONTOLOGY	General function prediction only,
GOTERM_BP_FAT	transcription, regulation of transcription, DNA-dependent, regulation of transcription, regulation of RNA metabolic process,
GOTERM_MF_FAT	zinc ion binding, ion binding, cation binding, metal ion binding, transition metal ion binding,
INTERPRO	Krueppel-associated box, Zinc finger, PHD-type, Zinc finger, C2H2-type, Zinc finger, C2H2-type/integrase, DNA-binding, Zinc finger, C2H2-like,
PIR_SUPERFAMILY	PIRSF005559:zinc finger protein ZFP-36,
SMART	PHD, KRAB, ZnF_C2H2,
SP_PIR_KEYWORDS	metal-binding, nucleus, repeat, Transcription, zinc,

Table 6: Classification of the genes used in my research using the Database for Annotation, Visualization and Integrated Discovery (DAVID) v6.7. (32, 33)

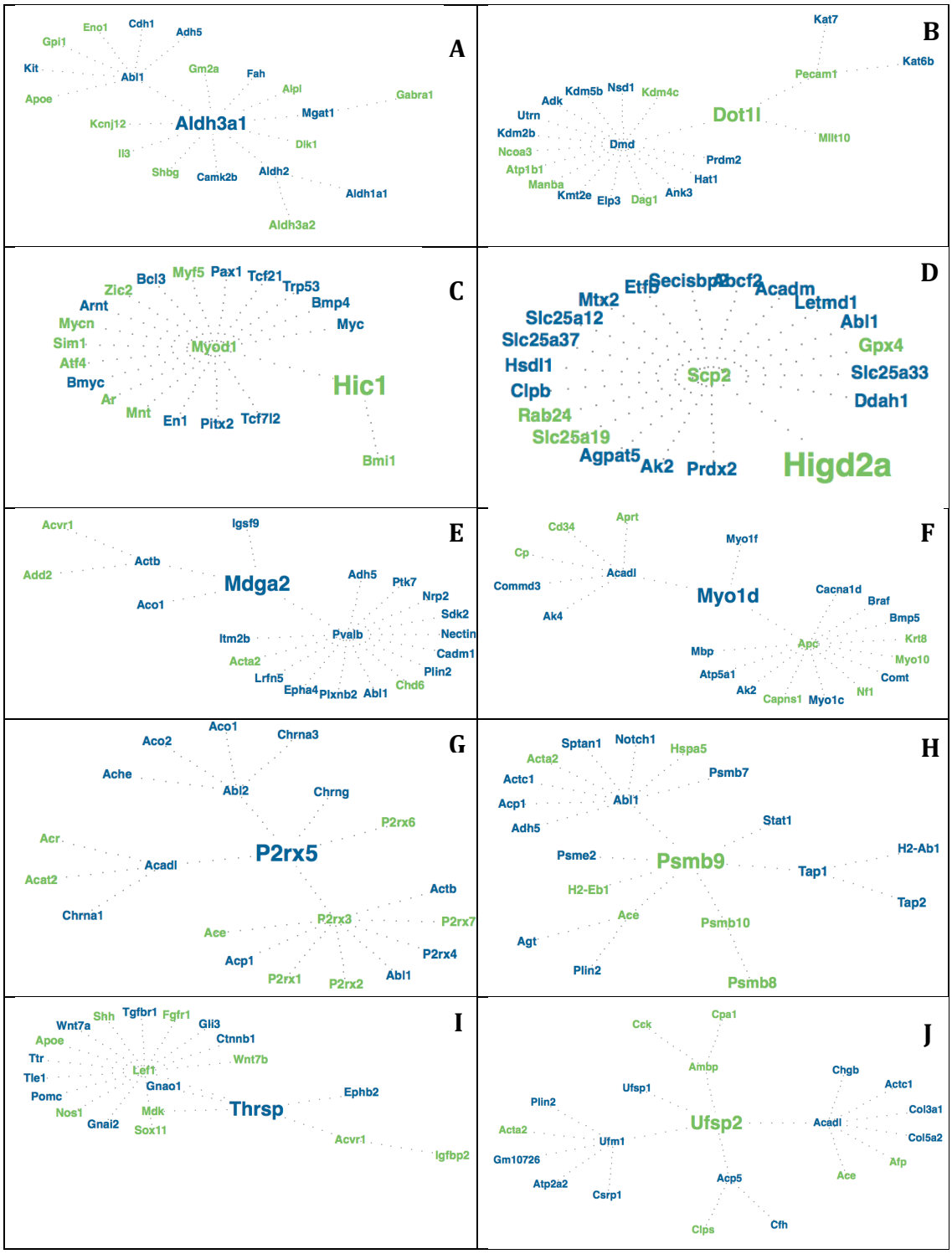
A
Eno1
Cdh1
Adh5
Gpi1
Kit
Abl1
Gm2a
Fah
Alpl
Gabra1
Apoe
Kcnj12
Aldh3a1
Mgat1
Il3
Dlk1
Shbg
Camk2b
Aldh2
Aldh1a1
Aldh3a2
B
Kat7
Kat6b
Pecam1
Kdm5b
Nsd1
Kdm4c
Adk
Utrn
Dot1l
Kdm2b
Mllt10
Dmd
Ncoa3
Prdm2
Atp1b1
Hat1
Manba
Kmt2e
Elp3
Dag1
Ank3
C
Bcl3
Myf5
Pax1
Tcf21
Zic2
Trp53
Arnt
Bmp4
Mycn
Myc
Sim1
Myod1
Atf4
Hic1
Bmyc
Ar
Mnt
En1
Pitx2
Tcf7l2
Bmi1
D
Etfb
Secisbp2
Abcf2
Acadm
Mtx2
Letmd1
Slc25a12
Abl1
Slc25a37
Gpx4
Hsdl1
Scp2
Slc25a33
Clpb
Ddah1
Rab24
Slc25a19
Agpat5
Ak2
Prdx2
Higd2a
E
Acvr1
Igsf9
Actb
Add2
Mdga2
Adh5
Ptk7
Aco1
Nrp2
Sdk2
Itm2b
Pvalb
Nectin
Acta2
Cadm1
Lrfn5
Plin2
Epha4
Plxnb2
Abl1
Chd6
F
Aprt
Cd34
Myo1f
Cp
Acadl
Commd3
Myo1d
Cacna1d
Braf
Ak4
Bmp5
Apc
Krt8
Mbp
Myo10
Atp5a1
Comt
Ak2
Capns1
Myo1c
Nf1
G
Aco1
Aco2
Chrna3
Ache
Abl2
Chrng
P2rx6
Acr
P2rx5
Acadl
Acat2
Actb
Chrna1
P2rx3
P2rx7
Ace
P2rx4
Acp1
P2rx1
P2rx2
Abl1
H
Sptan1
Notch1
Hspa5
Acta2
Psmb7
Actc1
Abl1
Acp1
Stat1
Adh5
H2-Ab1
Psme2
Psmb9
Tap1
H2-Eb1
Tap2
Ace
Psmb10
Agt
Plin2
Psmb8
I
Shh
Tgfbr1
Fgfr1
Wnt7a
Gli3
Apoe
Ctnnb1
Ttr
Wnt7b
Lef1
Tle1
Gnao1
Ephb2
Pomc
Thrsp
Mdk
Nos1
Gnai2
Sox11
Acvr1
Igfbp2
J
Cpa1
Cck
Ambp
Chgb
Ufsp1
Actc1
Plin2
Col3a1
Ufsp2
Acadl
Acta2
Col5a2
Ufm1
Afp
Gm10726
Ace
Acp5
Atp2a2
Csrp1
Clps
Cfh

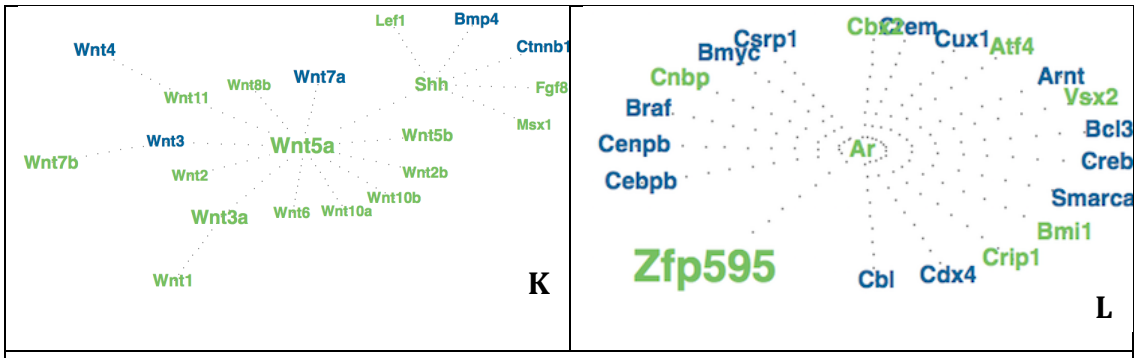

Figure 10: **Known genetic interactions for each of the candidate genes**. Figures developed using GeneCloud (Genecloud.org). A list of the top most related genes is plotted as a branching structure from the center. A secondary branch can occur if a gene in the graph is more related to a non-central gene than it is to the center gene. The font size of a branched gene indicates the relative strength of connection--always to the center gene.

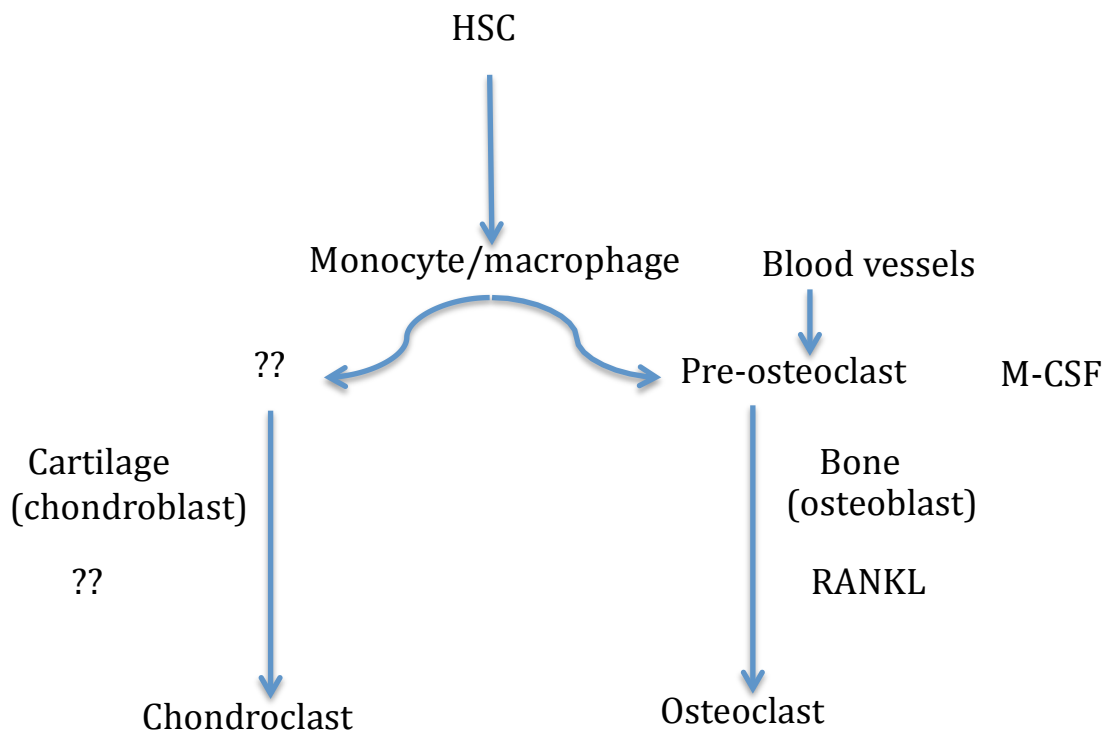

Figure 11: Model of Chondroclast and Osteoclast Lineage

REFERENCES

1. Pittenger MF, Mackay AM, Beck SC, Jaiswal RK, Douglas R, Mosca JD, Moorman MA, Simonetti DW, Craig S, Marshak DR. Multilineage potential of adult human mesenchymal stem cells. Science. 1999;284(5411):143-7. PubMed PMID: 10102814.
2. SF G. Osteogenesis: The Development of Bones (Developmental Biology). Sinauer Associates. 2000.
3. Mackie EJ, Ahmed YA, Tatarczuch L, Chen KS, Mirams M. Endochondral ossification: how cartilage is converted into bone in the developing skeleton. Int J Biochem Cell Biol. 2008;40(1):46-62. doi: 10.1016/j.biocel.2007.06.009. PubMed PMID: 17659995.
4. Mackie EJ, Tatarczuch L, Mirams M. The skeleton: a multi-functional complex organ: the growth plate chondrocyte and endochondral ossification. J Endocrinol. 2011;211(2):109-21. doi: 10.1530/JOE-11-0048. PubMed PMID: 21642379.
5. Arana-Chavez VE, Bradaschia-Correa V. Clastic cells: mineralized tissue resorption in health and disease. Int J Biochem Cell Biol. 2009;41(3):446-50. doi: 10.1016/j.biocel.2008.09.007. PubMed PMID: 18840541.
6. Roodman GD. Regulation of osteoclast differentiation. Ann N Y Acad Sci. 2006;1068:100-9. doi: 10.1196/annals.1346.013. PubMed PMID: 16831910.
7. Izawa T, Zou W, Chappel JC, Ashley JW, Feng X, Teitelbaum SL. c-Src links a RANK/alphavbeta3 integrin complex to the osteoclast cytoskeleton. Mol Cell Biol. 2012;32(14):2943-53. doi: 10.1128/MCB.00077-12. PubMed PMID: 22615494; PMCID: PMC3416198.
8. Tanaka Y, Nakayamada S, Okada Y. Osteoblasts and osteoclasts in bone remodeling and inflammation. Curr Drug Targets Inflamm Allergy. 2005;4(3):325-8. PubMed PMID: 16101541.
9. Zou W, Deselm CJ, Broekelmann TJ, Mecham RP, Vande Pol S, Choi K, Teitelbaum SL. Paxillin contracts the osteoclast cytoskeleton. J Bone Miner Res. 2012;27(12):2490-500. doi: 10.1002/jbmr.1706. PubMed PMID: 22807029; PMCID: PMC3494816.
10. Zhao H, Ito Y, Chappel J, Andrews NW, Teitelbaum SL, Ross FP. Synaptotagmin VII regulates bone remodeling by modulating osteoclast and osteoblast secretion. Dev Cell. 2008;14(6):914-25. doi: 10.1016/j.devcel.2008.03.022. PubMed PMID: 18539119; PMCID: PMC2480494.
11. DeSelm CJ, Miller BC, Zou W, Beatty WL, van Meel E, Takahata Y, Klumperman J, Tooze SA, Teitelbaum SL, Virgin HW. Autophagy proteins regulate the secretory component of osteoclastic bone resorption. Dev Cell. 2011;21(5):966-74. doi: 10.1016/j.devcel.2011.08.016. PubMed PMID: 22055344; PMCID: PMC3244473.
12. Wlodarski KH, Brodzikowska A, Kuzaka B. Are chondroclasts and osteoclasts identical? Folia Biol (Krakow). 2014;62(2):143-7. PubMed PMID: 25134344.
13. Ota N, Takaishi H, Kosaki N, Takito J, Yoda M, Tohmonda T, Kimura T, Okada Y, Yasuda H, Kawaguchi H, Matsumoto M, Chiba K, Ikegami H, Toyama Y. Accelerated cartilage resorption by chondroclasts during bone fracture healing in

osteoprotegerin-deficient mice. Endocrinology. 2009;150(11):4823-34. doi: 10.1210/en.2009-0452. PubMed PMID: 19819969.
14. Odgren PR, Witwicka H, Reyes-Gutierrez P. The cast of clasts: catabolism and vascular invasion during bone growth, repair, and disease by osteoclasts, chondroclasts, and septoclasts. Connect Tissue Res. 2016:1-14. doi: 10.3109/03008207.2016.1140752. PubMed PMID: 26818783.
15. Knowles HJ, Moskovsky L, Thompson MS, Grunhen J, Cheng X, Kashima TG, Athanasou NA. Chondroclasts are mature osteoclasts which are capable of cartilage matrix resorption. Virchows Arch. 2012;461(2):205-10. doi: 10.1007/s00428-012-1274-3. PubMed PMID: 22782381.
16. Nordahl J, Andersson G, Reinholt FP. Chondroclasts and osteoclasts in bones of young rats: comparison of ultrastructural and functional features. Calcif Tissue Int. 1998;63(5):401-8. PubMed PMID: 9799825.
17. Bettex-Galland M, Boillat C, Bettex M. Chondroclasts in osteoneogenesis. Tissue Cell. 1990;22(1):93-100. PubMed PMID: 2326791.
18. Clifton K SD, Gibson J, Lorenzo J, Hansen MF, Drissi H. Gene array analyses reveal distinct expression patterns in the osteoclast and chondroclast populations within a fracture callus. J Bone Mineral Res. 2012;27(Suppl 1):LB-MO13).
19. Smith N, Dong Y, Lian JB, Pratap J, Kingsley PD, van Wijnen AJ, Stein JL, Schwarz EM, O'Keefe RJ, Stein GS, Drissi MH. Overlapping expression of Runx1(Cbfa2) and Runx2(Cbfa1) transcription factors supports cooperative induction of skeletal development. J Cell Physiol. 2005;203(1):133-43. doi: 10.1002/jcp.20210. PubMed PMID: 15389629.
20. Gibson JD, Jakuba CM, Boucher N, Holbrook KA, Carter MG, Nelson CE. Single-cell transcript analysis of human embryonic stem cells. Integr Biol (Camb). 2009;1(8-9):540-51. doi: 10.1039/b908276j. PubMed PMID: 20023769.
21. Livak KJ, Schmittgen TD. Analysis of relative gene expression data using real-time quantitative PCR and the 2(-Delta Delta C(T)) Method. Methods. 2001;25(4):402-8. doi: 10.1006/meth.2001.1262. PubMed PMID: 11846609.
22. Gu J, Lu Y, Li F, Qiao L, Wang Q, Li N, Borgia JA, Deng Y, Lei G, Zheng Q. Identification and characterization of the novel Col10a1 regulatory mechanism during chondrocyte hypertrophic differentiation. Cell Death Dis. 2014;5:e1469. doi: 10.1038/cddis.2014.444. PubMed PMID: 25321476; PMCID: PMC4649528.
23. Zhu F, Friedman MS, Luo W, Woolf P, Hankenson KD. The transcription factor osterix (SP7) regulates BMP6-induced human osteoblast differentiation. J Cell Physiol. 2012;227(6):2677-85. doi: 10.1002/jcp.23010. PubMed PMID: 21898406; PMCID: PMC3241898.
24. Vu TH, Shipley JM, Bergers G, Berger JE, Helms JA, Hanahan D, Shapiro SD, Senior RM, Werb Z. MMP-9/gelatinase B is a key regulator of growth plate angiogenesis and apoptosis of hypertrophic chondrocytes. Cell. 1998;93(3):411-22. PubMed PMID: 9590175; PMCID: PMC2839071.
25. Kim HS, Lee NK. Gene expression profiling in osteoclast precursors by insulin using microarray analysis. Mol Cells. 2014;37(11):827-32. doi: 10.14348/molcells.2014.0223. PubMed PMID: 25377254; PMCID: PMC4255103.
26. Burington B, Barlogie B, Zhan F, Crowley J, Shaughnessy JD, Jr. Tumor cell gene expression changes following short-term in vivo exposure to single agent

chemotherapeutics are related to survival in multiple myeloma. Clin Cancer Res. 2008;14(15):4821-9. doi: 10.1158/1078-0432.CCR-07-4568. PubMed PMID: 18676754; PMCID: PMC3685184.
27. Arijs I, De Hertogh G, Lemaire K, Quintens R, Van Lommel L, Van Steen K, Leemans P, Cleynen I, Van Assche G, Vermeire S, Geboes K, Schuit F, Rutgeerts P. Mucosal gene expression of antimicrobial peptides in inflammatory bowel disease before and after first infliximab treatment. PLoS One. 2009;4(11):e7984. doi: 10.1371/journal.pone.0007984. PubMed PMID: 19956723; PMCID: PMC2776509.
28. Salaverria I, Philipp C, Oschlies I, Kohler CW, Kreuz M, Szczepanowski M, Burkhardt B, Trautmann H, Gesk S, Andrusiewicz M, Berger H, Fey M, Harder L, Hasenclever D, Hummel M, Loeffler M, Mahn F, Martin-Guerrero I, Pellissery S, Pott C, Pfreundschuh M, Reiter A, Richter J, Rosolowski M, Schwaenen C, Stein H, Trumper L, Wessendorf S, Spang R, Kuppers R, Klapper W, Siebert R, Molecular Mechanisms in Malignant Lymphomas Network Project of the Deutsche K, German High-Grade Lymphoma Study G, Berlin-Frankfurt-Munster NHLtg. Translocations activating IRF4 identify a subtype of germinal center-derived B-cell lymphoma affecting predominantly children and young adults. Blood. 2011;118(1):139-47. doi: 10.1182/blood-2011-01-330795. PubMed PMID: 21487109.
29. Lin A, Wang RT, Ahn S, Park CC, Smith DJ. A genome-wide map of human genetic interactions inferred from radiation hybrid genotypes. Genome Res. 2010;20(8):1122-32. doi: 10.1101/gr.104216.109. PubMed PMID: 20508145; PMCID: PMC2909575.
30. Mishra V, Sinha SK, Rajavashisth TB. Role of macrophage colony-stimulating factor in the development of neointimal thickening following arterial injury. Cardiovasc Pathol. 2016;25(4):284-92. doi: 10.1016/j.carpath.2016.04.003. PubMed PMID: 27135205.
31. Wada T, Nakashima T, Hiroshi N, Penninger JM. RANKL-RANK signaling in osteoclastogenesis and bone disease. Trends Mol Med. 2006;12(1):17-25. doi: 10.1016/j.molmed.2005.11.007. PubMed PMID: 16356770.
32. Huang da W, Sherman BT, Lempicki RA. Systematic and integrative analysis of large gene lists using DAVID bioinformatics resources. Nat Protoc. 2009;4(1):44-57. doi: 10.1038/nprot.2008.211. PubMed PMID: 19131956.
33. Huang da W, Sherman BT, Lempicki RA. Bioinformatics enrichment tools: paths toward the comprehensive functional analysis of large gene lists. Nucleic Acids Res. 2009;37(1):1-13. doi: 10.1093/nar/gkn923. PubMed PMID: 19033363; PMCID: PMC2615629.